Disparities in spatially variable gene calling highlight the need for benchmarking spatial transcriptomics methods.

Natalie Charitakis[1,2,3], Agus Salim[4,5], Adam T. Piers[1,3,6], Kevin I. Watt[1,3,7], Enzo R. Porrello[1,3,8,*], David A. Elliott[1,2,3,*], Mirana Ramialison[1,2,3,9*]

1 Murdoch Children's Research Institute, Royal Children's Hospital, Flemington Road, Parkville, Victoria, 3052, Australia
2 Department of Paediatrics, University of Melbourne, Grattan Street, Parkville, Victoria, 3010, Australia
3 Novo Nordisk Foundation Center for Stem Cell Medicine, Murdoch Children's Research Institute, Royal Children's Hospital, Flemington Road, Parkville, Victoria, 3052, Australia.
4 Melbourne School of Population and Global Health, University of Melbourne, Bouverie St, Carlton, Victoria, 3053, Australia
5 School of Mathematics and Statistics, University of Melbourne, Swanston Street, Parkville, Victoria, 3010, Australia
6 Melbourne Centre for Cardiovascular Genomics and Regenerative Medicine, The Royal Children's Hospital, Melbourne, Victoria, 3052, Australia
7 Department of Diabetes, Monash University, Alfred Centre, Commercial Road, Melbourne, Victoria, 3004, Australia
8 Department of Anatomy and Physiology, University of Melbourne, Grattan Street, Parkville, Victoria, 3010, Australia
9 Australian Regenerative Medicine Institute, Monash University, Clayton, Victoria, 3800, Australia
* co-senior authors

Co-corresponding Authors:
mirana.ramialison@mcri.edu.au
Mirana Ramialison
david.elliott@mcri.edu.au
David Elliott
enzo.porrello@mcri.edu.au
Enzo Porrello

Abstract

Identifying spatially variable genes (SVGs) is a key step in the analysis of spatially resolved transcriptomics (SRT) data. SVGs provide biological insights by defining transcriptomic differences within tissues, which was previously unachievable using RNA-sequencing technologies. However, the increasing number of published tools designed to define SVG sets currently lack benchmarking methods to accurately assess performance. This study compares results of 5 purpose-built packages for SVG identification across 8 public and 3 simulated datasets and highlights discrepancies between results. Additional tools for generation of simulated data and development of benchmarking methods are required to improve methods for identifying SVGs.

Background

Spatially resolved transcriptomics (SRT) captures variations in gene expression across tissues (1–7). Computational methods for analysis of SRT data are being established (8–11). The goal of SRT analysis pipelines is the robust and reliable identification of spatially variable genes (SVGs) within tissue sections (12,13). SVGs are defined as having expression levels across a tissue that covary in a location specific manner(12,14). Published methods for SVG identification employ different mathematical models aiming to capture biological truth (12,13,15–23). Benchmarking analysis tools is needed to ensure the reliability of processed data matches or supersedes that of similar technologies such as single-cell (sc) RNA-Seq (24,25).

Here, we compared the performance of five packages SpatialDE(12), SPARK-X(15), Seurat(18), SpaGCN(17) and scGCO(16). Eight SRT datasets from healthy and cancerous

formalin fixed (FF) and formalin-fixed paraffin embedded (FFPE) tissues generated with 10X Visium technology (26,27) were used alongside three simulated datasets. Our analysis reveals discrepancies in SVGs identified by each package highlighting the urgent need for a standardised benchmark dataset (or ground truth) for SRT.

Results and Discussion

Comparing SVGs predicted by commonly used packages, we found that the numbers of SVGs identified differed by one to two orders of magnitude across the same tissue for all eight investigated datasets (Fig. 1A & Additional Files 2-4, S1-3). For example, in the FF Endometrial Adenocarcinoma Ovarian Tissue dataset, the number of predicted SVGs ranged from 87 to 3707 (Fig. 1A). For 7/8 datasets, SpaGCN consistently identifies the fewest number of SVGs, while SpatialDE identifies the greatest number (Fig. 1A & Additional Files 2-4, S1-3). Since Seurat ranks highly variable genes (HVGs) by how dependent their expression is on spatial location, the number of SVGs identified is consistent across datasets (Fig. 1A & Additional Files 2-4, S1-3)(28).

To understand the disparity in the number of SVGs reported, we hypothesised that methods used to correct for type I error might influence the number of SVGs predicted. While Seurat and SpaGCN produce lists of SVGs with no associated p-values, SpatialDE, scGCO and SPARK-X report a q-value/ FDR for all genes. Methods that do not supply associated p-values report the lowest number of SVGs across datasets (Fig. 1A & Additional Files 2-4, S1-3).

Across all datasets, the number of common SVGs identified between the 5 packages are consistent, but minimal. However, common SVGs display an expression pattern that aligns with spatial correlation suggesting that they are *bona fide* SVGs (Fig. 1B).

Next, to assess the significance of small overlap between predicted SVGs, the ranked lists of SVGs provided by SpatialDE, scGCO and SPARK-X were compared across datasets using a Wilcoxon signed rank test. We observed differences in the SVG ranking across the tested packages, indicating that the lack of overlap is statistically significant (Additional File 11, Table S3, Fig. 1C & Additional Files 5-7, S4-6). Differences between reported q-values for a single gene between packages are visualised in Figure 1C and S2-4.

We investigated the impact on downstream analysis resulting from these discordant results by comparing gene ontology (GO) enrichment analysis conducted using SVGs predicted by each software within the same tissue (Fig. 1D & Additional File 8, S7). We observed non-overlapping parent terms between datasets in the top 10 over-represented GO terms (Fig. 1D & Additional File 8, S7). These results suggest that gene sets predicted by each package do not overlap functionally. This suggests restricting further analysis to SVGs can bias downstream interpretation of results, especially if there is a risk of a large percentage of false positives (FP).

Despite the discrepancies, SVGs identified by all packages within the same dataset display an expression pattern aligned with a clear spatial correlation. An example is *JCHAIN,* which is expressed in macrophages in endometrial tissue and associated with adenocarcinoma (Fig 1B) (29–31). This observation indicates that patterns with a stronger signal to noise ratio are identified by all methods.

Inconsistencies in the results between different packages may therefore be explained by the differences in FP rates by the different algorithms, rather than false negatives rates. To investigate this, we generated four negative control datasets from two publicly available datasets. For each, two versions of negative controls were generated - [1] where spatial coordinates are permuted and [2] where spatial coordinates and columns of gene expression

matrix are permuted. For all negative control datasets generated from the FF Left Ventricle, Seurat, scGCO and SPARK-X identified no SVGs, indicating an ability to distinguish signal from noise. SpaGCN identified <10 SVGs. SpatialDE identified 4 SVGs when both spatial coordinates and columns of the gene expression matrix are permuted and 2953 in the other dataset. For negative control datasets generated from FFPE prostate randomising only spatial coordinates, SpatialDE identified 632 SVGs and SpaGCN identified 232. All other packages returned no results. When spatial coordinates and gene expression values were randomised, SpatialDE was the only package to identify SVGs (713). Patterns of the top SVGs identified by SpatialDE are visualised in Fig. S6 and lack a strong spatial pattern. This would indicate that SpatialDE is prone to introducing FP into a dataset compared to other packages. However, the original SVGs identified by SpatialDE and the result in Fig. 1D suggest the top ranked SVGs labelled by SpatialDE in real data display a signal consistent with that of a SVG.

In addition to differences in FP rates, results generated from different packages applied to the same dataset may be due to the different assumptions regarding the underlying distributions of gene expression and effectiveness of normalisation methods (Additional File 11, Table S1). Negative binomial distributions can successfully model sequencing-based methods that employ unique molecular identifiers (UMIs) (32). While certain packages implement their own normalisation method, there is no guarantee that data pre-processed using a separate workflow will have been normalised to fit the assumptions of gene distribution held by a particular package (12,18). Once methods for generating simulated SRT datasets with different underlying distributions of gene expression are published, the effect this has on identifying SVGs needs to be investigated thoroughly. Further simulated datasets will help identify discrepancies in SVGs within the same dataset as certain mathematical models may detect specific expression patterns.

There are many caveats to generating simulated datasets with known patterns of gene expression with efforts focused on simulating data with defined cell types (33–40). One simulated dataset generated using SPARK-X was tested on SPARK-X and SpatialDE only (as the output dataset proved incompatible with the other packages). Within this dataset, SPARK-X identifies 1003 SVGs and SpatialDE 1009 (Additional file 10, Fig. S9). SPARK-X and SpatialDE identified all true positives. SPARK-X identifies 6 unique SVGs, while SpatialDE 12 unique SVGs (Additional file 10, Fig. S9).

Conclusions

While different mathematical models for detecting SVGs produce varied results when applied to the same tissue, and across tissues and biological conditions, SVGs with a strong spatial covariance are consistently identified. This indicates that differences between methods do not bias performance in a particular tissue or biological condition. While SVGs with a strong signal are detected by multiple packages, additional methods for generating simulated datasets containing known SVG expression pattern are required to accurately determine the extent to which packages may introduce FP (13,14). Only 3 of the tested packages produced q-value ranked gene lists, thus differences in FP rates could confound comparisons of results across packages. Furthermore, as the resolution of the Visium technology platform results in sequencing of >10 cells within a single spot, the presence of heterogenous cell types could complicate accurate identification of SVGs. Spots with a homogeneous cell type population will be enriched for an expression profile of a single cell type, whereas spots with a heterogenous cell composition will be more challenging to define due to inherent transcriptional variation. Increased resolution may present challenges in terms of

computational performance and the mathematical difficulties of dealing with highly sparse datasets. As SVG identification becomes an integral part of the computational analysis of SRT and datasets grow, a subset of SVGs could be used in preference over the entire dataset for downstream analysis (such as highly variable genes in scRNA-Seq analysis). Introducing noise may hamper key downstream steps in understanding spatially restricted disease states as well as novel targets for treatment (41,42). The development of simulated datasets for benchmarking current and novel methods for SVG identification will allow for accurate determination of the spatially restricted transcriptional differences that manifest as biological outcomes during development and disease.

Methods

Five packages were selected for comparison: SpatialDE(12), SPARK-X(15), Seurat (18), SpaGCN(17) and scGCO(16), which each employ a different mathematical model to identify SVGs. Each package was tested on 8 publicly available, V1 Chemistry Visium datasets generated from healthy and cancerous human tissues (Table S2). The filtered output files and imaging data from the Space Ranger v1.0.0 pipeline was downloaded, filtered, and pre-processed using Scanpy v1.8.1 (43). Default parameters were used, except with SpaGCN where the radius and number of domains was calculated for each dataset. Using the FF Left Ventricle and FFPE Prostate datasets as inputs, two negative control datasets were generated in each instance by 1) independently randomising the x and y spot coordinates to remove spatial correlation and 2) repeating the aforementioned steps but randomising each column in the gene expression matrix to ensure any overall association was removed.

References

1. Marx V. Method of the Year: spatially resolved transcriptomics. Nat Methods. 2021 Jan 1;18(1):9–14.
2. Asp M, Bergenstråhle J, Lundeberg J. Spatially Resolved Transcriptomes-Next Generation Tools for Tissue Exploration. Bioessays. 2020 Oct 1;42(10).
3. Waylen LN, Nim HT, Martelotto LG, Ramialison M. From whole-mount to single-cell spatial assessment of gene expression in 3D. Communications Biology 2020 3:1. 2020 Oct 23;3(1):1–11.
4. Ståhl PL, Salmén F, Vickovic S, Lundmark A, Navarro JF, Magnusson J, et al. Visualization and analysis of gene expression in tissue sections by spatial transcriptomics. Vol. 353, Science. American Association for the Advancement of Science; 2016. p. 78–82.
5. Larsson L, Frisén J, Lundeberg J. Spatially resolved transcriptomics adds a new dimension to genomics. Vol. 18, Nature Methods. Nature Research; 2021. p. 15–8.
6. Moses L, Pachter L. Museum of spatial transcriptomics. Nature Methods 2022 19:5. 2022 Mar 10;19(5):534–46.
7. Williams CG, Lee HJ, Asatsuma T, Vento-Tormo R, Haque A. An introduction to spatial transcriptomics for biomedical research. Genome Medicine 2022 14:1. 2022 Jun 27;14(1):1–18.
8. Zeng Z, Li Y, Li Y, Luo Y. Statistical and machine learning methods for spatially resolved transcriptomics data analysis. Genome Biology 2022 23:1. 2022 Mar 25;23(1):1–23.
9. Noel T, Wang QS, Greka A, Marshall JL. Principles of Spatial Transcriptomics Analysis: A Practical Walk-Through in Kidney Tissue. Front Physiol. 2022 Jan 6;12:2317.
10. Liu B, Li Y, Zhang L. Analysis and Visualization of Spatial Transcriptomic Data. Front Genet. 2022 Jan 27;0:2852.
11. Dries R, Chen J, Rossi N del, Khan MM, Sistig A, Yuan GC. Advances in spatial transcriptomic data analysis. Genome Res. 2021 Oct 1;31(10):1706–18.
12. Svensson V, Teichmann SA, Stegle O. SpatialDE: Identification of spatially variable genes. Nat Methods. 2018;15(5).

13. Li K, Yan C, Li C, Chen L, Zhao J, Zhang Z, et al. Computational elucidation of spatial gene expression variation from spatially resolved transcriptomics data. Mol Ther Nucleic Acids. 2022 Mar 8;27:404–11.
14. Walker BL, Cang Z, Ren H, Bourgain-Chang E, Nie Q. Deciphering tissue structure and function using spatial transcriptomics. Communications Biology 2022 5:1. 2022 Mar 10;5(1):1–10.
15. Zhu J, Sun S, Zhou X. SPARK-X: non-parametric modeling enables scalable and robust detection of spatial expression patterns for large spatial transcriptomic studies. Genome Biol. 2021 Dec 1;22(1):1–25.
16. Zhang K, Feng W, Wang P. Identification of spatially variable genes with graph cuts. bioRxiv. bioRxiv; 2018. p. 491472.
17. Hu J, Li X, Coleman K, Schroeder A, Ma N, Irwin DJ, et al. SpaGCN: Integrating gene expression, spatial location and histology to identify spatial domains and spatially variable genes by graph convolutional network. Nature Methods 2021 18:11. 2021 Oct 28;18(11):1342–51.
18. Satija R, Farrell JA, Gennert D, Schier AF, Regev A. Spatial reconstruction of single-cell gene expression data. Nat Biotechnol. 2015 May 12; 33(5):495–502.
19. Xu Y, McCord RP. CoSTA: unsupervised convolutional neural network learning for spatial transcriptomics analysis. BMC Bioinformatics. 2021 Dec 1;22(1):1–26.
20. Hao M, Hua K, Zhang X. SOMDE: A scalable method for identifying spatially variable genes with self-organizing map. bioRxiv. 2021;
21. Weber LM, Saha A, Datta A, Hansen KD, Hicks SC. nnSVG: scalable identification of spatially variable genes using nearest-neighbor Gaussian processes. bioRxiv. 2022 May 16;2022.05.16.492124.
22. Sun S, Zhu J, Zhou X. Statistical analysis of spatial expression patterns for spatially resolved transcriptomic studies. Nature Methods 2020 17:2. 2020 Jan 27;17(2):193–200.
23. Jiang X, Xiao G, Li Q. A Bayesian modified Ising model for identifying spatially variable genes from spatial transcriptomics data. Stat Med. 2022 Jul 24;
24. Adil A, Kumar V, Jan AT, Asger M. Single-Cell Transcriptomics: Current Methods and Challenges in Data Acquisition and Analysis. Front Neurosci. 2021 Apr 22;15:398.

25. Chen G, Ning B, Shi T. Single-cell RNA-seq technologies and related computational data analysis. Front Genet. 2019;10(APR):317.
26. Palla G, Fischer DS, Regev A, Theis FJ. Spatial components of molecular tissue biology. Nature Biotechnology 2022 40:3. 2022 Feb 7;40(3):308–18.
27. Li K, Yan C, Li C, Chen L, Zhao J, Zhang Z, et al. Computational elucidation of spatial gene expression variation from spatially resolved transcriptomics data. Mol Ther Nucleic Acids. 2022 Mar 8;27.
28. Hoffman P, Satija Lab. Analysis, visualization, and integration of spatial datasets with Seurat • Seurat.
29. Dun EC, Hanley K, Wieser F, Bohman S, Yu J, Taylor RN. Infiltration of tumor-associated macrophages is increased in the epithelial and stromal compartments of endometrial carcinomas. International Journal of Gynecological Pathology. 2013 Nov;32(6):576–84.
30. The Human Protein Atlas [Internet]. [cited 2022 Sep 12]. Available from: https://www.proteinatlas.org/
31. Wang W, Vilella F, Alama P, Moreno I, Mignardi M, Isakova A, et al. Single-cell transcriptomic atlas of the human endometrium during the menstrual cycle. Nature Medicine 2020 26:10. 2020 Sep 14;26(10):1644–53.
32. Svensson V. Droplet scRNA-seq is not zero-inflated. Nature Biotechnology 2020 38:2. 2020 Jan 14;38(2):147–50.
33. Ma Y, Zhou X. Spatially informed cell-type deconvolution for spatial transcriptomics. Nat Biotechnol. 2022 May 2;
34. Miller BF, Huang F, Atta L, Sahoo A, Fan J. Reference-free cell type deconvolution of multi-cellular pixel-resolution spatially resolved transcriptomics data. Nature Communications 2022 13:1. 2022 Apr 29;13(1):1–13.
35. Dong R, Yuan GC. SpatialDWLS: accurate deconvolution of spatial transcriptomic data. Genome Biol. 2021 Dec 1;22(1):1–10.
36. Cable DM, Murray E, Zou LS, Goeva A, Macosko EZ, Chen F, et al. Robust decomposition of cell type mixtures in spatial transcriptomics. Nature Biotechnology 2021 40:4. 2021 Feb 18;40(4):517–26.
37. Elosua-Bayes M, Nieto P, Mereu E, Gut I, Heyn H. SPOTlight: seeded NMF regression to deconvolute spatial transcriptomics spots with single-cell transcriptomes. Nucleic Acids Res. 2021 May 21 ; 49(9):e50–e50.

38. Kleshchevnikov V, Shmatko A, Dann E, Aivazidis A, King HW, Li T, et al. Cell2location maps fine-grained cell types in spatial transcriptomics. Nature Biotechnology 2022 40:5. 2022 Jan 13;40(5):661–71.
39. Bae S, Choi H, Lee DS. spSeudoMap: Cell type mapping of spatial transcriptomics using unmatched single-cell RNA-seq data. bioRxiv. 2022 May 10;2022.05.09.491104.
40. Song Q, Su J. DSTG: deconvoluting spatial transcriptomics data through graph-based artificial intelligence. Brief Bioinform. 2021 Sep 2;22(5):1–13.
41. Navarro JF, Croteau DL, Jurek A, Andrusivova Z, Yang B, Wang Y, et al. Spatial Transcriptomics Reveals Genes Associated with Dysregulated Mitochondrial Functions and Stress Signaling in Alzheimer Disease. iScience. 2020 Oct 23 ; 23(10):101556.
42. Wang Y, Ma S, Ruzzo WL. Spatial modeling of prostate cancer metabolic gene expression reveals extensive heterogeneity and selective vulnerabilities. Scientific Reports 2020 10:1. 2020 Feb 26;10(1):1–14.
43. Wolf FA, Angerer P, Theis FJ. SCANPY: Large-scale single-cell gene expression data analysis. Genome Biol. 2018 Feb 6;19(1):15.

Figure Legends

Figure 1. Discrepancies between SVGs in a dataset annotated by five different packages. **A)** Upset plots displaying the distinct intersections of SVGs identified in FF Endometrial Adenocarcinoma Ovarian Tissue dataset when analysed with SpaGCN, scGCO, Seurat, SPARK-X and SpatialDE. **B)** Gene ontology enrichment results using SVGs identified by each package as inputs. **C)** Sorted q-values from SpatialDE results across the FF Left Ventricle datasets plotted against SPARK-X q-values for the same gene. **D)** Pattern of expression of JCHAIN, a SVG identified by all 5 packages in FF Endometrial Adenocarcinoma Ovarian Tissue. Spots representing the capture regions of the Visium slide are overlayed on accompanying histological image.

Figure 2. **Expression patterns of SVGs identified by all tested packages in a single dataset.** **A)** Pattern of expression of ALB, a SVG identified by all 5 packages in FF Invasive Ductal

Carcinoma Breast Tissue. **B)** Pattern of expression of ACTA1, a SVG identified by all 5 packages in FF Healthy Left Ventricle. **C)** Pattern of expression of BTG2, a SVG identified by all 5 packages in FFPE Healthy Prostate. **D)** Pattern of expression of TACSTD2, a SVG identified by all 5 packages in FFPE Invasive Ductal Carcinoma Breast Tissue.

Declarations

Ethic approval and consent to participate

NA

Consent for publication

NA

Availability of data and materials

The input files for the Visium data used in this study are available from the 10X Genomics website. Examples of the data pre-processing and analysis to identify SVGs on a single dataset for each of the five packages can be found on Github at the repository Ramialison-Lab/Disparities_in_SVG_Calling.

Additional file 1: additional_file.pdf

Supplementary Methods

Additional file 2: additional_file2.pdf

Figure S1. Distinct overlap of SVGs identified by different combinations of the five tested packages. A) FF cerebellum. B) FF lymph node. C) FFPE adenocarcinoma prostate.

Additional file 3: additional_file3.pdf

Figure S2. Distinct overlap of SVGs identified by different combinations of the five tested packages. A) FF invasive ductal carcinoma breast tissue. B) FF healthy left ventricle. C) FFPE Healthy Prostate.

Additional file 4: additional_file4.pdf

308 Figure S3. Distinct overlap of SVGs identified by different combinations of the five tested
309 packages. A) FFPE Invasive Ductal Carcinoma Breast Tissue.
310
311 **Additional file 5**: additional_file5.pdf
312 Figure S4. Comparison of ranked SpatialDE q-values against gene-matched SPARK-X q-
313 values of all genes generated from each dataset. Order of plots repeats across all datasets. A)
314 FF cerebellum. B) FF lymph node. C) FFPE adenocarcinoma prostate. D) FF invasive ductal
315 carcinoma breast tissue. E) FFPE healthy prostate. F) FFPE invasive ductal carcinoma breast
316 tissue. G) FF endometrial adenocarcinoma ovarian tissue.
317
318 **Additional file 6:** additional_file6.pdf
319 Figure S5. Comparison of ranked SpatialDE q-values against gene-matched scGCO q-values
320 of all genes generated from each dataset. Order of plots repeats across all datasets. A) FF
321 cerebellum. B) FF lymph node. C) FFPE adenocarcinoma prostate. D) FF invasive ductal
322 carcinoma breast tissue. E) FFPE healthy prostate. F) FFPE invasive ductal carcinoma breast
323 tissue. G) FF endometrial adenocarcinoma ovarian tissue. H) FF healthy left ventricle.
324
325 **Additional file 7:** additional_file7.pdf
326 Figure S6. Comparison of ranked SPARK-X q-values against gene-matched scGCO q-values
327 of all genes generated from each dataset. Order of plots repeats across all datasets. A) FF
328 cerebellum. B) FF lymph node. C) FFPE adenocarcinoma prostate. D) FF invasive ductal
329 carcinoma breast tissue. E) FFPE healthy prostate. F) FFPE invasive ductal carcinoma breast
330 tissue. G) FF endometrial adenocarcinoma ovarian tissue. H) FF healthy left ventricle.
331
332 **Additional file 8:** additional_file8.pdf
333 Figure S7. Gene ontology enrichment results using SVGs identified by each package as inputs
334 across datasets. A) FF cerebellum. B) FF lymph node. C) FFPE adenocarcinoma prostate. D)

335 FF invasive ductal carcinoma breast tissue. E) FF healthy left ventricle. F) FFPE healthy
336 prostate. G) FFPE invasive ductal carcinoma breast tissue.
337
338 **Additional file 9:** additional_file9.pdf
339 Figure S8. Top SVG identified by SpatialDE in negative simulated datasets generated by A)
340 Randomising coordinates of FF Left Ventricle dataset. B) Randomising counts and coordinates
341 of FF Left Ventricle dataset. C) Randomising coordinates of FFPE Prostate dataset. D)
342 Randomising counts and coordinates of FFPE Prostate dataset.
343
344 **Additional file 10:** additional_file10.pdf
345 Figure S9. Upset plot of results generated from running SPARK-X and SpatialDE on simulated
346 data with known pattern of SVGs.
347
348 **Additional file 11:** additional_file11.xlsx
349 Contains Tables 1-3. Table S1) Packages included for identification of SVGs in benchmarking
350 study. Table S2) Overview of publicly available 10X Visium datasets to be included in
351 benchmarking process. FF indicates tissues that are fresh frozen and FFPE indicates tissues
352 that are formalin-fixed paraffin-embedded. The filtered output files and imaging data from the
353 Space Ranger v1.0.0, v1.2.0 or V1.3.0 pipeline were downloaded for each dataset. Table S3)
354 Reported statistic and associated p-value from each combination of pairwise comparison of
355 results between SpatialDE, SPARK-X and scGCO when reported p-values were compared
356 using the Wilcoxon signed rank test.

Competing Interests

ERP is a cofounder, scientific advisor, and holds equity in Dynomics, a biotechnology company focused on the development of heart failure therapeutics. The other authors report no conflicts.

Funding

The authors acknowledge grant and fellowship support from the National Health and Medical Research Council of Australia (E.R.P., D.A.E., M.R.), the Stafford Fox Medical Research Foundation (E.R.P, D.A.E.), and the Royal Children's Hospital Foundation (E.R.P., D.A.E.). The Novo Nordisk Foundation Center for Stem Cell Medicine (E.R.P., D.A.E., M.R.) is supported by Novo Nordisk Foundation grants (NNF21CC0073729). The Murdoch Children's Research Institute is supported by the Victorian Government's Operational Infrastructure Support Program.

Authors' contributions

N.C. performed experiments with contribution from A.S. on statistical design; N.C., A.S., A.T.P., K.I.W, E.R.P., D.A.E., M.R. designed experiments; N.C., K.I.W, D.A.E., M.R. wrote the manuscript with input from A.S. and E.R.P.

Acknowledgements

The authors would like to thank David Powell, Gordon Smyth and Matthew Ritchie for their feedback, and Michael See for use of his code in generating plots.

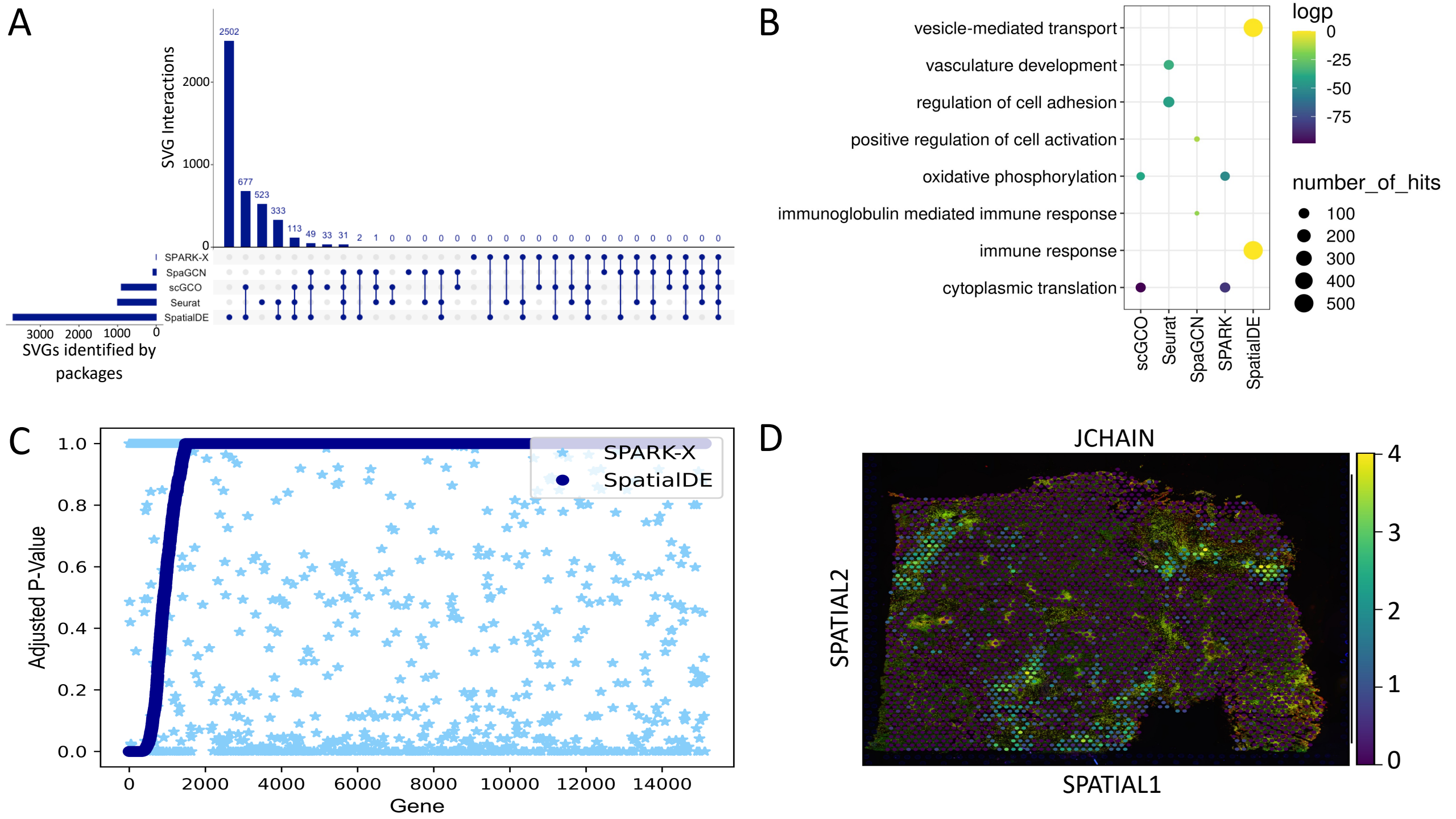
A
SVG Interactions
2502
677
523
333
113
49
33
31
2
1
0
2000
1000
0
SPARK-X
SpaGCN
scGCO
Seurat
SpatialDE
3000
2000
1000
0
SVGs identified by packages
B
vesicle-mediated transport
vasculature development
regulation of cell adhesion
positive regulation of cell activation
oxidative phosphorylation
immunoglobulin mediated immune response
immune response
cytoplasmic translation
scGCO
Seurat
SpaGCN
SPARK
SpatialDE
logp
0
-25
-50
-75
number_of_hits
100
200
300
400
500
C
Adjusted P-Value
1.0
0.8
0.6
0.4
0.2
0.0
SPARK-X
SpatialDE
0
2000
4000
6000
8000
10000
12000
14000
Gene
D
JCHAIN
SPATIAL2
SPATIAL1
4
3
2
1
0

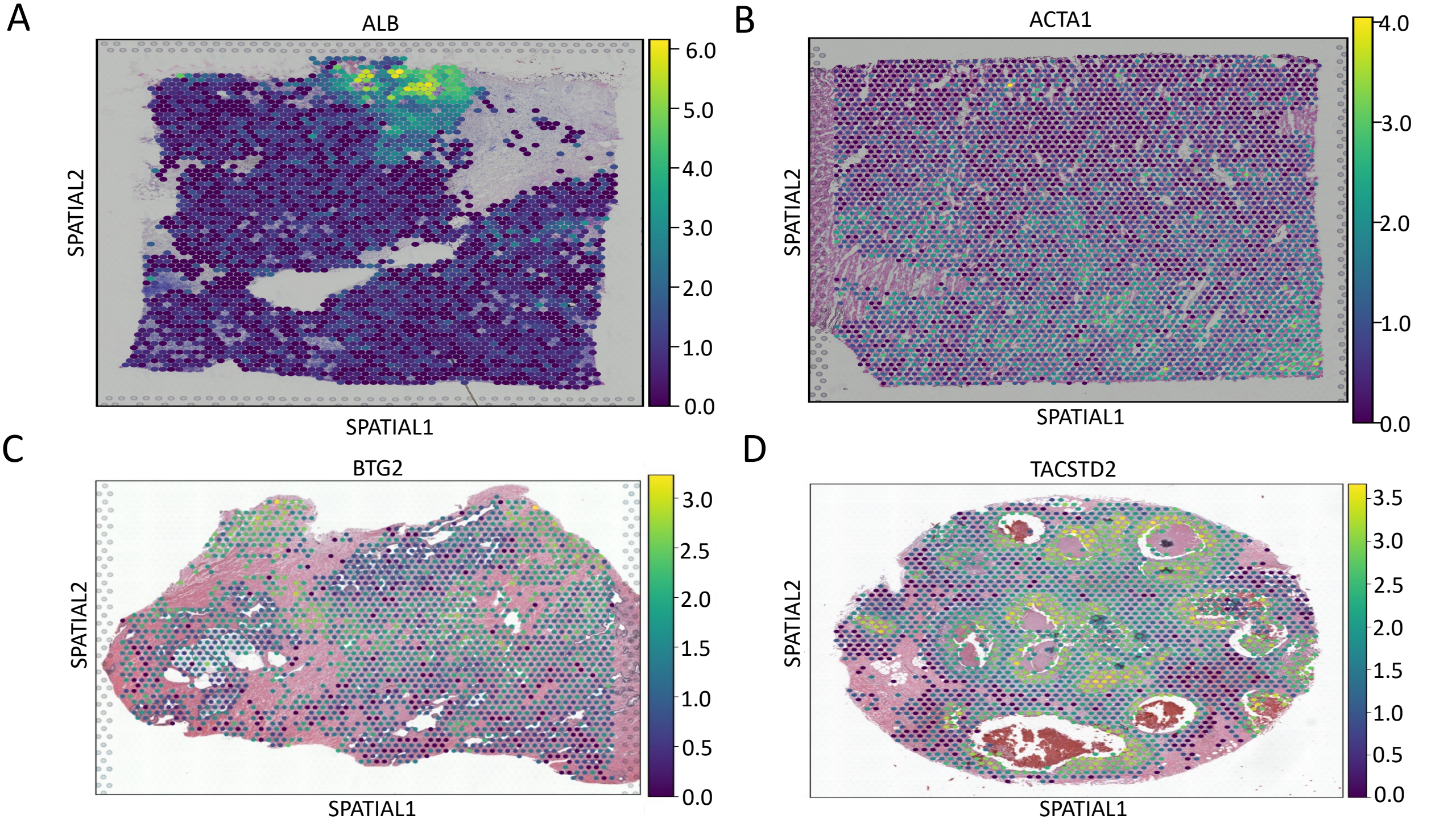
A
ALB
SPATIAL2
SPATIAL1
6.0
5.0
4.0
3.0
2.0
1.0
0.0
B
ACTA1
SPATIAL2
SPATIAL1
4.0
3.0
2.0
1.0
0.0
C
BTG2
SPATIAL2
SPATIAL1
3.0
2.5
2.0
1.5
1.0
0.5
0.0
D
TACSTD2
SPATIAL2
SPATIAL1
3.5
3.0
2.5
2.0
1.5
1.0
0.5
0.0